The 8th European Congress on Computational Methods in Applied Sciences and Engineering
ECCOMAS Congress 2022
5 – 9 June 2022, Oslo, Norway

FLUID-STRUCTURE INTERACTION SIMULATION OF A WIRE-WRAPPED TUBE ARRAY USING OVERSET GRIDS

HENRI DOLFEN[1], DIETER VAN HAUWERMEIREN[1], AXEL BRAL[1] AND JORIS DEGROOTE[1,2]

[1] Department of Electromechanical, Systems and Metal Engineering
Ghent University
Sint-Pietersnieuwstraat 41, 9000, Ghent, Belgium
e-mail: henri.dolfen@ugent.be, www.fsi.ugent.be

[2] Flanders Make
Ghent, Belgium

Key words: Overset grids, Wire-wrapped tube bundles, Nuclear fuel assemblies, Computational Fluid Dynamics, Fluid-structure interaction

Abstract. Axial flows in tube bundle geometries are omnipresent in nuclear power plants, including fuel assemblies and heat exchangers. The tubes are often long and slender which makes them susceptible to flow-induced vibrations. Current reactor research investigates the use of wires helicoidally wound around each rod, to preserve their mutual distance. This poses new challenges for numerical simulations. The wire-wrapped geometry is complex, among other things due to small gaps, making the meshing process complicated and cumbersome.

This research explores the use of overset grids for such wire-wrapped tube bundles. This meshing method allows grids to overlap and the flow solution is interpolated between the different grids, providing more freedom for meshing. In this case the approach consists of making one grid for a single tube with a wire, termed the component mesh, and placing this grid in a so-called background mesh that takes into account other geometrical features (e.g. the bundle duct). In the case of bundles, the same tube mesh can be repeated several times without additional meshing effort, regardless of the bundle size.

The approach is verified using 4 cases found in literature, using the same component mesh either one or multiple times for each case, thus reducing the meshing effort to a minimum thanks to the freedom and re-usability overset offers. The first two cases involve a fluid-structure interaction simulation of a single wire-wrapped tube in a cylindrical domain, the first one simulating a steady deformation and the second one a free vibration of the tube. Good agreement with results in literature was found. The latter two cases are Computational Fluid Dynamics simulations of a 7-pin and 19-pin bundle in a hexagonal duct, and excellent agreement with literature results was obtained. The overset approach was proven beneficial for simulating wire-wrapped bundle geometries: with largely reduced effort the same predictive capabilities can be obtained and potentially even extended.

1 INTRODUCTION

Wire-wrapped tube arrays are a geometry often applied in the design of nuclear reactor cores [1], the wire being helically wound around the fuel pins of the assembly to preserve the distance between adjacent pins. This spacing is an important parameter which controls the nuclear reaction rate and heat transfer. The cases simulated in this research were based on the nuclear reactor core design of the Multi-purpose hYbrid Research Reactor for High-tech Applications (MYRRHA) [2] which is currently under design. The main goal of this research is to investigate whether the use of an overset grid can be a significant improvement regarding the meshing time and complexity for Computational Fluid Dynamics (CFD) and Fluid-Structure Interaction (FSI) simulations of a wire-wrapped tube array, of which the basic layout is shown in Figure 1.

The overset (or Chimera) grid technique is a composite meshing technique that was developed by NASA following the 1986 Space Shuttle Challenger disaster. At that time, the meshing capabilities were not able to capture all geometric features of the Space Shuttle and therefore a better meshing tool was necessary to accurately predict its aerodynamics. Therefore, NASA developed the overset grid technique and employed it to improve the Space Shuttle's design [3]. The basic principle can be seen in Figure 2. Instead of creating a single, coherent computational domain, the mesh consists of a series of overlapping meshes. These do not have to be conformal with each other, which allows for an added flexibility to construct a mesh around more complex geometries such as a wire-wrapped tube. The mesh constructed around the more complex geometry or object is usually called the component mesh whereas the mesh with which it overlaps is usually defined as the background mesh.

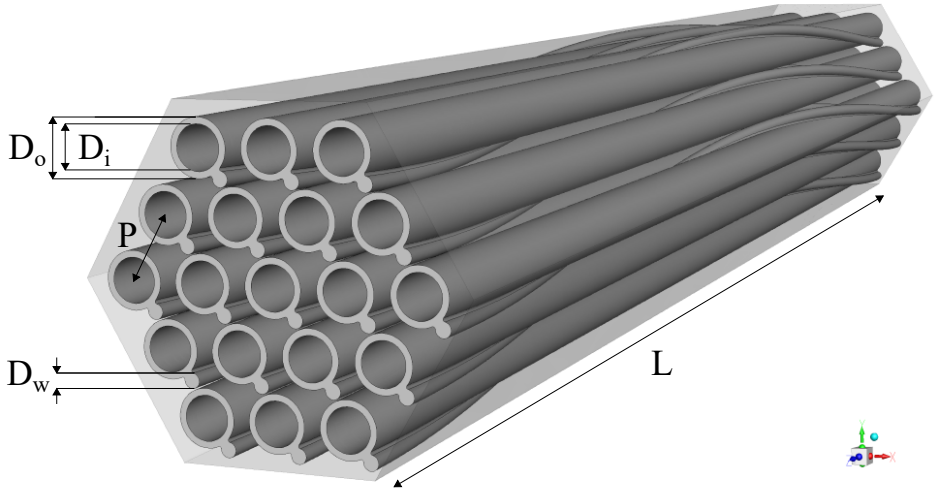

Figure 1: A 19-pin wire-wrapped tube bundle geometry. The inner tube diameter D_i, outer diameter D_o, wire diameter D_w, pin-to-pin pitch P and bundle length L are indicated, the latter being equal to one helical pitch in this example.

Overset grids have two clear advantages over the use of single grids. First, no geometric constraints are imposed on the overset boundary (see Figure 2), thereby increasing the mesh

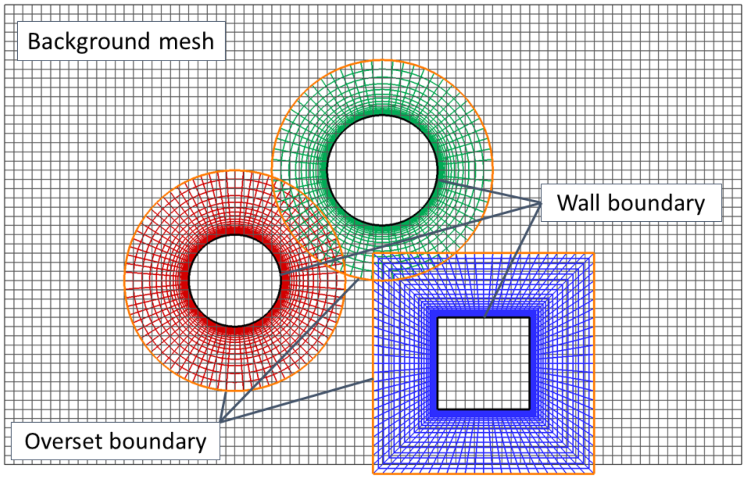

Figure 2: Illustration of the overset idea. Background mesh and three embedded component meshes with overset boundary condition. From Pözlbauer et al. [4].

design freedom compared to traditional grids. A second advantage, which specifically applies to tube arrays, is the reusability of the component meshes. When adapting the tube bundle's size, the same component mesh can be used for any number of tubes whereas for a single grid approach, a new mesh has to be generated for each bundle size. The added meshing flexibility of using overset grids combined with the reusability of the component mesh are therefore promising properties that motivate this research.

The added flexibility comes at a computational cost. Each grid needs to receive flow information, implying that information has to be exchanged between the different grids in the overlapping region. This is done by selecting certain cells and giving them the task of engaging in this inter-grid communication. These particular cells are called donor and receptor cells, depending on the task they perform. Donor cells will provide flow information to the receptor cells so they should be close to each other (albeit in a different grid). Creating these donor-receptor pairs and ensuring that every receptor cell is paired to a donor cell is done by so-called donor search algorithms. This search algorithm is largely responsible for the increased computational cost compared to single-grid approaches. Especially in a fluid-structure interaction simulation this can be a substantial computational cost, as the donor searching has to be repeated as the grids deform.

2 METHODOLOGY

The study consists of four simulation cases summarized in Table 1. For each case, the results using overset grids are compared with results found in literature for which a single-grid approach was used, serving as a validation benchmark for the overset results.

As can be seen from the table, case 1 and 2 are FSI simulations. This means that besides the CFD model, also a structural model will be discussed as well as the method coupling them together. Case 3 and 4 test the accuracy of the flow results on different bundle sizes, simultaneously displaying the modularity of the approach.

Table 1: Benchmark cases used to study the effectiveness and applicability of the overset mesh.

	Description	Benchmark
Case 1	Steady FSI of 1 fuel pin	Steady-state displacement from De Santis and Shams [1]
Case 2	Unsteady FSI of 1 fuel pin	Decaying vibration displacement from De Santis and Shams [1]
Case 3	Steady CFD of 7-pin bundle	Pressure drop from Cheng–Todreas correlation [5] Velocity field from Brockmeyer et al. [6]
Case 4	Steady CFD of 19-pin bundle	Velocity field from Doolaard et al. [7]

2.1 Flow model

As this paper has a specific focus on the meshing of the wire-wrapped tube, this will be elaborately covered in the next section, after which the more general CFD settings are discussed.

2.1.1 Mesh generation

The component mesh for the four cases is made with Ansys ICEM CFD. The tube's outer diameter is equal to $6.55 \times 10^{-3}\ m$ and the wire diameter is equal to $1.8 \times 10^{-3}\ m$. It is a block-structured mesh and the number of divisions applied to each different block are shown in Figure 3a. Also grading is applied: G denotes geometric grading, in which the subsequent cell sizes form a geometric series from one side of the edge to the other and B denotes bi-geometric grading, which utilizes the same cell size progression, but symmetric around the middle of the edge. The cell-to-cell growth factor is taken equal to 1.1 everywhere grading is used. This results in a number of cells in the cross-sectional plane (shown in Figure 3b) equal to 8190, while for the three-dimensional mesh it depends on the length of the rod, since different lengths are used for the different cases. To prevent mesh singularities at the line contact between rod and wire, the wire is connected to the tube by means of a straight segment of $0.04 \times 10^{-3}\ m$, divided in 9 (graded) cells, see the detail in Figure 3b. The mesh obtained in the cross-sectional plane is extruded in axial direction and the entire component mesh is twisted afterwards by modifying the nodal coordinates with a Python script. This is only possible thanks to the overset technique, for which the shape of the overset boundary does not matter. The meshing of a complex 3D domain has thus been simplified to meshing a 2D shape contained in an arbitrarily shaped outer domain.

The design of the structured background meshes is straightforward. For the first two cases, it has an annular shape (not shown). The third and fourth case use a hexagonally shaped background mesh defining the casing of the fuel assembly. As mentioned in the introduction, overset meshing involves a donor-search step, during which cells of each grid are selected for communication with the other grids (the so-called donor-receptor pairs). The result of this is shown for the 7-pin bundle (case 3) in Figure 4, with the donor cells indicated in red and the receptor cells in green. The receptor cells demarcate a zone within which the solution is obtained, so basically they are boundary conditions to this domain. Cells inside of this zone are called solve cells, some of which are donor cells to the overlapping mesh. The ones that do not have another role are indicated in yellow. Cells outside this zone are not required to obtain a

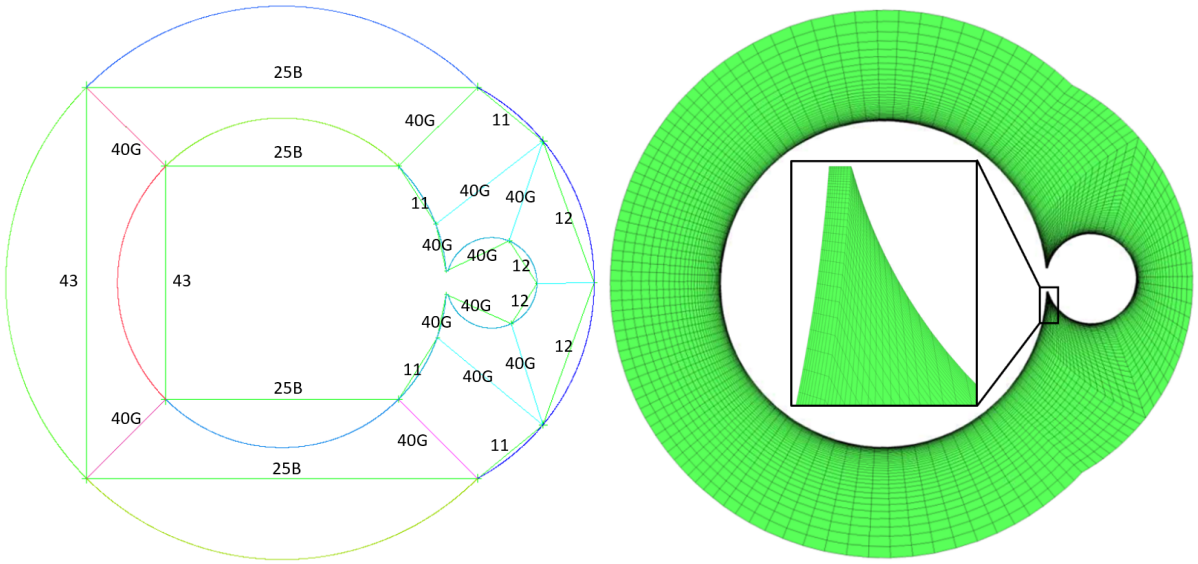

(a) (b)

Figure 3: (a) Block structure of the component mesh (G and B denoting geometric and bi-geometric grading respectively and the numbers indicating the divisions in each edge) and (b) cross-sectional view the resulting component mesh around the wire-wrapped tube.

solution and are deactivated, they are named dead cells. The total amount of cells used in the simulation is thus smaller than the sum of the cells of all grids participating. It can be seen from Figure 4b that a very large percentage of the background mesh consists of dead cells, because the component meshes have sufficient overlap to cover the entire inner region. This is taken into account for the background grid for the 19-pin bundle (not shown), where only the outer ring covering the edge subchannels is meshed.

Case 3 is a 7-rod bundle in a hexagonal casing with a side length of 14.67×10^{-3} m, case 4 a 19-pin bundle in a hexagonal casing of 23.12×10^{-3} m. The tube-to-tube pitch, which is defined as the distance between the centers of neighboring tubes, is equal to 8.45×10^{-3} m. This results in a minimum distance between the wire and tube of two neighboring pins of 0.1×10^{-3} m. This is an important factor to take into account, because the different meshes need sufficient overlap, which means enough layers have to be present in the first 0.1×10^{-3} m. This restricts the cell sizes at the wall to the extent that they will be in the viscous sublayer, thus the meshes are constructed such that the y^+ is close to 1 everywhere. This would have been the near-wall mesh design of choice also without this practical consideration, since the validation cases chosen for this paper also use wall-resolved meshes. It should be noted that the benchmark papers for case 3 and 4 employ a wire diameter of 1.75×10^{-3} m, which is slightly different than the one used here. To maintain the same minimal gap, the pin-to-pin pitch and hexagonal duct diameter have also slightly been adjusted compared to the benchmarks.

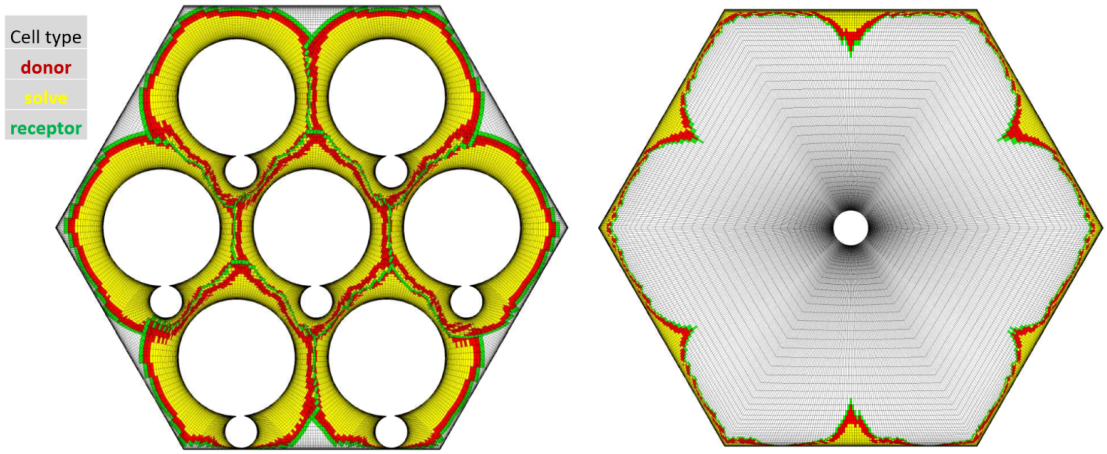

(a) (b)

Figure 4: Cell types for the (a) component mesh and (b) background mesh for the 7-pin bundle. Donor cells are shown in green, general solve cells in yellow and receptor cells in red. Uncolored cells are dead cells.

2.1.2 Setup

The flow solver used for this research is Ansys Fluent 2019R3. In all cases, a Reynolds-Averaged Navier–Stokes (RANS) approach is used, with the k-ω SST turbulence model. The working fluid is lead bismuth eutectic (LBE), having a density of 10364 kg/m^3 and a dynamic viscosity of 1.938×10^{-3} $Pa \cdot s$ at 300 $°C$. The boundary conditions at inlet and outlet for all four cases are respectively a constant velocity inlet and pressure outlet condition. The first two cases include FSI and therefore dynamic mesh zones have to be defined. As overset grids are used, only the component mesh has to deform.

2.2 Structural model

The Computational Solid Mechanics (CSM) package used for this work is Dassault Systèmes Abaqus 6.14. The mesh is shown in Figure 5. The wall thickness is 0.51×10^{-3} m and the wire helical pitch is equal to 0.265 m. The material is steel with a Young's modulus of 200 GPa and a Poisson ratio equal to 0.3. Furthermore, all cells are second-order 3D solid elements. The tube's circumference is divided into 36 elements whereas 3 divisions are made in the thickness direction. The circumference of the wire is divided into 26 cells. The mesh is extruded and twisted in axial direction using 200 divisions, similarly as has been done for the component geometry, to obtain a length of 0.7 m. The boundary conditions for the tube are defined as clamped at the upstream end ($z = 0$ m) and pinned at the downstream end ($z = 0.7$ m). The setup for the structural model was based as much as possible on the model used in De Santis and Shams [1]. However, not all the simulation parameters could be inferred, such that some uncertainty exists whether the model used for this research is accurately replicated. It was found that the in-vacuo eigenfrequencies of the structural model did not agree exactly with the ones published by De Santis and Shams [1], with differences up to 10%. The implementation of the pinned boundary

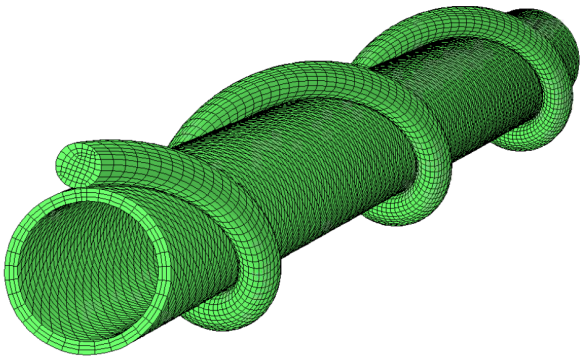

Figure 5: Finite element mesh of the wire-wrapped fuel pin.

condition was not unambiguously defined, this could be a large source of uncertainty. Therefore, quantitative differences in results are possible but these do not necessarily disprove the validity of the overset grid approach but rather show a difference in computational models.

2.3 Fluid-structure interaction

The structural model is coupled to the flow model in a partitioned way [8], i.e. by exchanging the pressure and wall shear loads from the flow solution and displacements from the structural solution at their mutual interface. This means the solvers itself can be considered black-boxes. This procedure is implemented in the lightweight open-source Python coupling code CoCoNuT[1] developed at Ghent University. The coupling is done implicitly, meaning that the solver solutions are iteratively communicated back-and-forth, until some convergence criterion is reached, in this case the L_2-norm of the displacement residual, which has to drop 7 orders of magnitude. The convergence is enhanced by the IQN-ILS coupling algorithm (interface quasi-Newton with inverse Jacobian of the residual from a least-squares model) [9].

3 RESULTS

3.1 Case 1: steady FSI of a single wire-wrapped tube

In this first case, a steady FSI simulation of a single wire-wrapped tube is performed. The case setup is based on the work of De Santis and Shams [1]. A wire-wrapped tube with a length of 0.7 m is placed in a cylindrical channel of diameter 42.6×10^{-3} m. A uniform velocity of 2 m/s is applied at the inlet. Because of the asymmetric geometry of the wire-wrapped configuration, the forces exerted by the flow will push the tube out of its centerline position. The goal in this case is to determine the steady-state centerline displacement of the tube along its length and compare it with the displacements obtained by De Santis and Shams [1].

The comparison between these results is displayed in Figure 6. The presence of the local extrema are captured accurately for the overset case. The quantitative difference can be ascribed to the uncertainties concerning the structural model as previously described, as they seem to originate mainly from the pinned boundary condition at the downstream side. The results are approximated sufficiently well to conclude that the overset technique proved to be effective.

[1] `https://pyfsi.github.io/coconut`

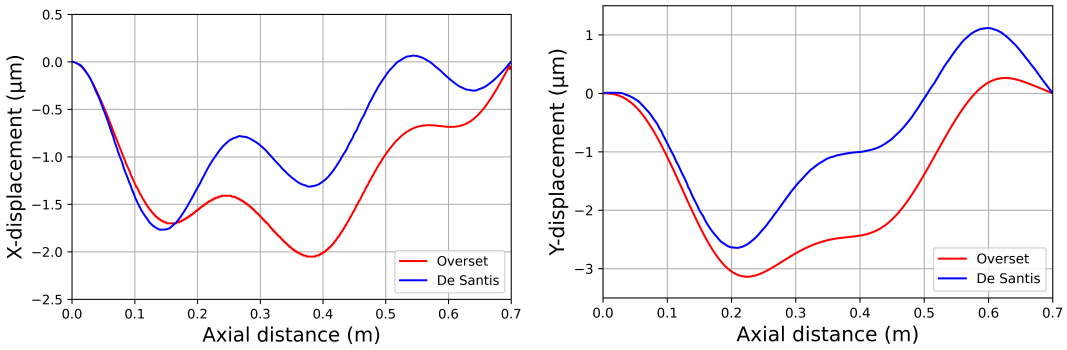

(a) (b)

Figure 6: A comparison of (a) the x-displacement and (b) the y-displacement of the centerline between the overset case and the results obtained in De Santis and Shams [1].

3.2 Case 2: unsteady FSI of a single wire-wrapped tube

The second case is an unsteady FSI simulation, also replicating the work of De Santis and Shams [1]. An impulsive force is applied at the center of the wire-wrapped tube which induces a vibration that decays due to fluid damping [1]. The goal is to extract the modal parameters from this vibration and compare these with the results of the benchmark. The same flow conditions apply as for case 1 and the total time simulated is 0.5 s with a time step of 2.5×10^{-4} s.

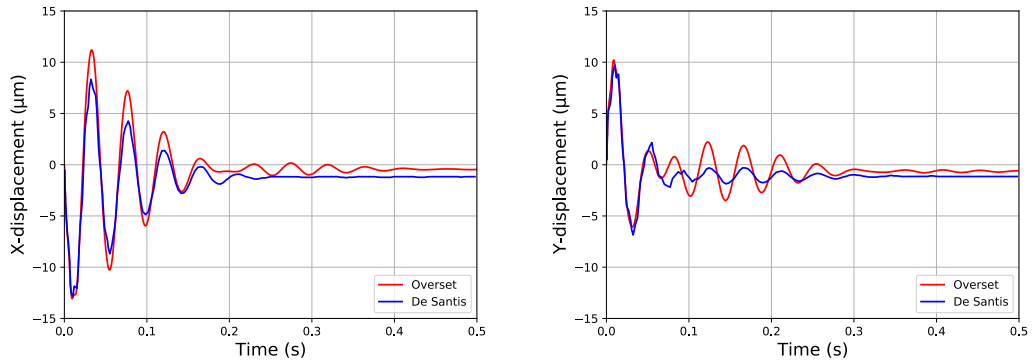

(a) (b)

Figure 7: A comparison of (a) the x-displacement and (b) the y-displacement of the middle of the tube between the overset case and the results obtained in De Santis and Shams [1] as a function of time. The overset results are scaled in vertical direction with a factor of 0.25 for visualization purposes.

The comparison between x- and y-displacements of a cross-section at the center of the tube is shown in Figure 7. In order to facilitate visual comparison, the results found with overset are scaled by a factor of approximately 0.25 to match the amplitudes obtained in the benchmark (the

Table 2: Comparison of the oscillation frequency of x- and y-displacements between overset and De Santis and Shams [1].

	Frequency (Hz)	
	x-displacement	y-displacement
De Santis and Shams [1]	23.36	23.47
Overset	23.36	23.04
Error (%)	0.0	1.8

magnitude of the impulsive load was not mentioned in De Santis and Shams [1]). The amplitude difference is not expected to influence the modal characteristics significantly. For the y-direction, the results of this research show a decrease in amplitude followed by an increase whereas the results of De Santis and Shams [1] do not show this to the same extent. A similar phenomenon is seen for the x-displacement but to a smaller extent. This is possibly caused by mode coupling, where energy is transferred from one mode to another. The difference in results can possibly be ascribed to the uncertainties regarding the structural model and simulation setup used in De Santis and Shams [1]. Nonetheless, the amplitude decay is well captured and the displacements settle down at the steady-state values found in the previous case (not visible in Figure 7 due to the scaling). Moreover, the oscillation frequencies of both cases agree well with each other, a comparison can be found in Table 2. These are obtained by fitting the characteristic equation (containing the frequency) of a decaying vibration to the data of the centerline, as was done in earlier work on vibrating tubes [1, 10]. From these results, the overset technique has proven valid for the unsteady case as well.

3.3 Case 3: steady CFD of a 7-pin wire-wrapped tube bundle

In the third setup a 7-pin tube bundle is investigated, to demonstrate the modularity of the component mesh. The mesh is shown in Figure 4 illustrating how the component meshes are organized and overlap with the background mesh. The domain of interest has a length of 1 wire pitch. To ensure data is extracted in a region of developed flow, an entrance region with a length of 0.025 m is added before the domain of interest. Also an outflow domain of 0.063 m is added, where the component mesh is not twisted. To validate the results of this case, two benchmarks were used.

The first validation consists of calculating the pressure drop using the correlation of Cheng and Todreas [5] and comparing these results with the CFD results. For this, several simulations were performed with different inlet velocities ranging from 1.0 m/s to 1.8 m/s. As can be seen in Figure 8a, the agreement between the correlation and the CFD results is excellent, with a maximal error of 5.3 % at 1.0 m/s.

A second validation is done by a comparison between contour plots for velocity magnitude from the overset results and (time-averaged) large-eddy simulation (LES) results of Brockmeyer et al. [6]. In that work periodic boundary conditions at inlet and outlet are used, whereas the current research used a velocity inlet and pressure outlet. This choice is motivated by the incompatibility of overset grids and periodic boundary conditions in ANSYS Fluent 2019R3, but the precursor domain should enhance the flow development. Figure 8b shows a contour plot

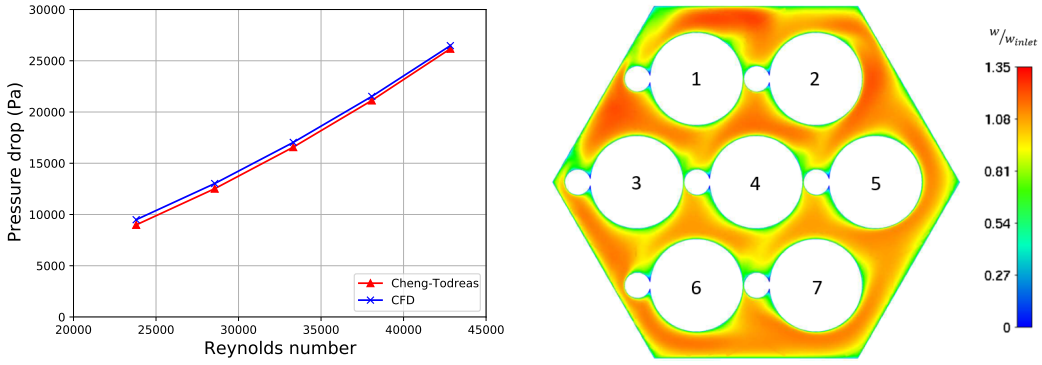

(a) (b)

Figure 8: (a) A comparison of the pressure drop between the value resulting from the Cheng and Todreas correlation and the CFD results. (b) Contour plot of the axial velocity at an axial distance of 0.194 m from the start of the domain of interest.

of the axial velocity nondimensionalized by the inlet velocity, which was 1.8 m/s in this case. The cross-section is taken at $z = 0.194$ m. Comparing this plot to the one found in the work of Brockmeyer et al. [6] (not shown), a good qualitative agreement was found.

3.4 Case 4: steady CFD of a 19-pin wire-wrapped tube bundle

The fourth case is similar to the third case but with 19 tubes instead of 7 and a velocity of 1.8 m/s. Again the domain of interest has a length of one wire pitch, which is 0.262 m in this case. Note that this length is different than for case 1 and 2, but the implementation is trivial as the entire component mesh is twisted, so it just comes down to reducing this twist from 0.265 $m/360°$ to 0.262 $m/360°$. Here a more quantitative comparison than in case 3 is the objective, with the benchmark being the results found in Doolaard et al. [7]. In this paper, several research institutions including Ghent University (UGent) participated to simulate the flow along a wire-wrapped tube bundle using a RANS-based approach. For this case, a developed velocity profile, which was extracted from a preliminary simulation, is applied at the inlet. This is done to approximate the periodic boundary conditions used by Doolaard et al. [7]. Besides that, a precursor domain was still used as was done for the previous case, as well as some additional length behind the region of interest. The total number of cells for the mesh is 44 287 200, of which 37 834 187 are solve cells. The mesh of the UGent contribution to the benchmark contains 35 412 498 cells, which are mostly tetrahedrons except for 10 boundary layers.

To compare the current research with the benchmark results obtained by UGent, the three velocity components are taken along a horizontal line as shown in Figure 9a. The line is drawn at an axial coordinate of $z = 0.210$ m which is 80% of the pitch. The velocity components for the overset case and the results of Doolaard et al. [7] are shown in Figure 9b, Figure 9c and Figure 9d. The same conclusion can be made for all three plots as the velocities of the overset case and reference paper agree well with each other. Combined with the results obtained in the previous case, this validates the use of overset for tube bundles.

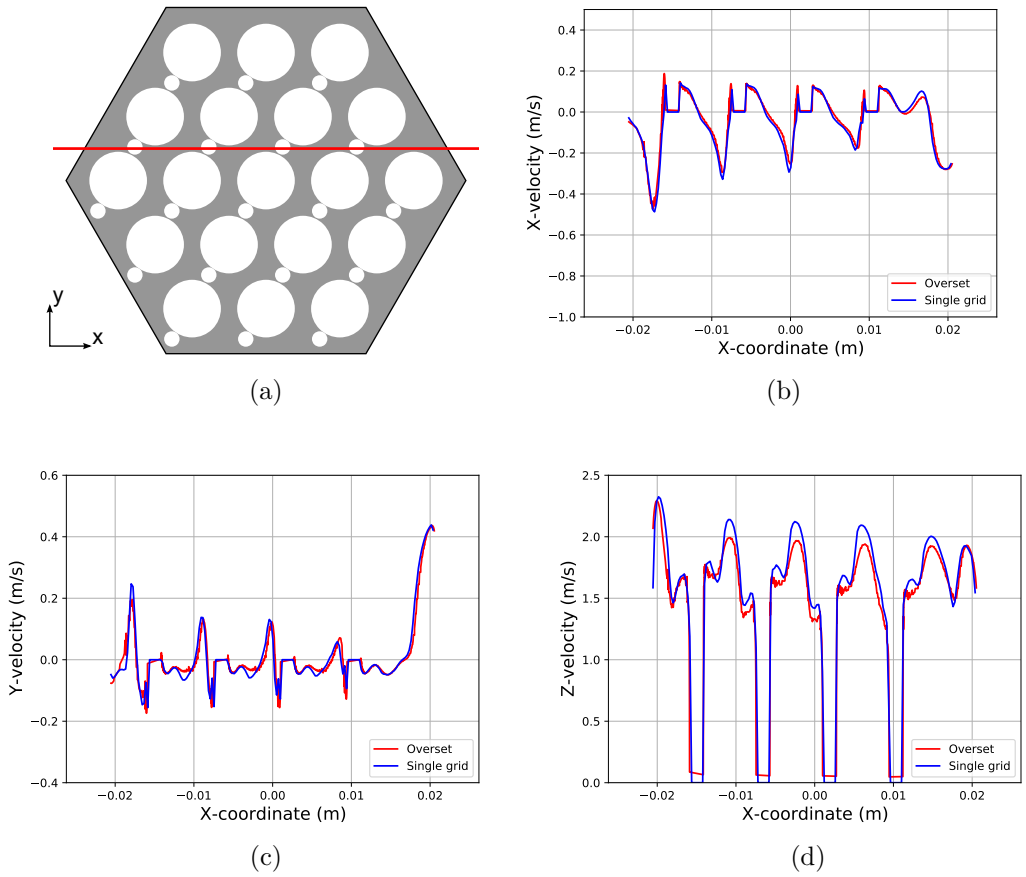

(a) (b) (c) (d)

Figure 9: (a) Cross-section of the 19-pin bundle geometry at $z = 0.210\ m$ with the line for data extraction indicated in red (at $y = 3.63731 \times 10^{-3}\ m$). A comparison of (b) the x-velocity, (c) the y-velocity and (d) the z-velocity. The single grid data is extracted from the UGent contribution to the work of Doolaard et al. [7].

4 CONCLUSIONS

The applicability of overset meshing for wire-wrapped tubes has been demonstrated by employing it in both a steady (case 1) and unsteady (case 2) FSI simulation and comparing displacement results to a reference case from literature. After that, the research was extended to bundles: a 7-pin (case 3) and 19-pin (case 4) bundle using the same component mesh were used in steady CFD simulations and the results were compared qualitatively and quantitatively to benchmark results from literature and empirical correlations. As for all four cases good agreement was observed, it can be concluded that the overset technique is a valid and useful alternative for single-grid approaches. The reusability of the component mesh was demonstrated for a 7-pin and 19-pin wire-wrapped tube bundle. It can thus be concluded that the meshing process of wire-wrapped tube geometries can be significantly simplified and also extended to any desired number of pins.

Future work includes extending the predictive capabilities, by investigating whether the overset technique can be used to simulate flow-induced vibrations in bundles, where contact between the tubes can occur.

5 ACKNOWLEDGMENT

This project has received funding from the European Union's Horizon Europe research and innovation programme under grant agreement No 101060826.

REFERENCES

[1] De Santis, D. and Shams, A. Analysis of flow induced vibrations and static deformations of fuel rods considering the effects of wire spacers and working fluids. *J. Fluids. Struct.* (2019) **84**:440–465.

[2] Engelen, J., Aït Abderrahim, H., Baeten, P., De Bruyn, D., and Leysen, P. MYRRHA: Preliminary front-end engineering design. *Int. J. Hydrog.* (2015) **40(44)**: 15137–15147.

[3] Chiu, I.-T., *On computations of the integrated space shuttle flowfield using overset grids.* PhD Thesis, Iowa State University (1990).

[4] Pölzlbauer, P., Kümmel, A., Desvigne, D. and Breitsamter, C. Numerical Investigation of an Optimized Rotor Head Fairing for the RACER Compound Helicopter in Cruise Flight. *Aerospace* (2021) **8(3)**:66.

[5] Chen, S.K., Chen, Y.M. and Todreas, N.E. The upgraded Cheng and Todreas correlation for pressure drop in hexagonal wire-wrapped rod bundles. *Nucl. Eng. Des.* (2018) **335**:356–373.

[6] Brockmeyer, L., Merzari, E., Solberg, J. and Hassan, Y. One-way coupled simulation of FIV in a 7-pin wire-wrapped fuel pin bundle. *Nucl. Eng. Des.* (2020) **356**:110367.

[7] Doolaard, H., Shams, A., Roelofs, F., Van Tichelen, K., Keijers, S., De Ridder, J., Degroote, J., Vierendeels, J., Di Piazza, I., Marinari, R., Merzari, E., Obabko, A. and Fischer, P. CFD benchmark for a heavy liquid metal fuel assembly. *NURETH-16*. Chicago, IL, August 30-September 4, 2015.

[8] Degroote, J.. Partitioned Simulation of Fluid-Structure Interaction. *Arch. Comput. Methods Eng.* (2013) **20(3)**:185–238.

[9] Degroote, J., Bathe, K.-J. and Vierendeels, J. Performance of a new partitioned procedure versus a monolithic procedure in fluid–structure interaction. *Comput. Struct.* (2009) **87(11)**:793–801.

[10] De Ridder, J., Degroote, J., Van Tichelen, K., Schuurmans, P., and Vierendeels, J. Modal characteristics of a flexible cylinder in turbulent axial flow from numerical simulations. *J. Fluids. Struct.* (2013). **43**:110–123.